

DESY 95-215
December 1995
hep-ph/9603205

PAIR PRODUCTION OF NEUTRAL HIGGS PARTICLES IN GLUON–GLUON COLLISIONS

T. PLEHN¹, M. SPIRA^{2*} AND P. M. ZERWAS¹

¹ Deutsches Elektronen–Synchrotron DESY, D–22603 Hamburg, FRG

² II. Institut für Theoretische Physik[†], D–22761 Hamburg, FRG

Abstract

Pair production processes of neutral Higgs particles will allow us to study the trilinear Higgs couplings at future high-energy colliders. Several mechanisms give rise to multi-Higgs final states in hadron interactions. In the present paper we investigate Higgs pair production in gluon–gluon collisions. After recapitulating pair production in the Standard Model, the analysis of the cross sections is carried out in detail for the neutral Higgs particles in the minimal supersymmetric extension.

*Address after Jan.1,1996: TH Division, CERN, CH-1211 Geneva 23, Switzerland

[†]Supported by Bundesministerium für Bildung und Forschung (BMBF), Bonn, under Contract 05 6 HH 93P (5), and by EU Program *Human Capital and Mobility* through Network *Physics at High Energy Colliders* under Contract CHRX-CT93-0357 (DG12 COMA).

1 Introduction

The reconstruction of the Higgs potential is an experimental *prima facie* task to establish the Higgs mechanism as the basic mechanism for generating the masses of the fundamental particles. This task requires the measurement of the self-couplings of the Higgs particles.

In the Standard Model (SM) [1] the trilinear and the quartic couplings of the physical Higgs particle H are uniquely fixed if the Higgs mass is known.

In the minimal supersymmetric extension of the Standard Model (MSSM), a large variety of couplings exists among the members h, H, A, H^\pm of the Higgs quintet [2]. [h and H are the light and heavy CP-even Higgs bosons¹, A is the CP-odd (pseudoscalar) Higgs boson, and H^\pm is the charged Higgs pair.] While general two-doublet models contain three mass parameters and seven real self-couplings in CP conserving theories, the Higgs self-couplings are fixed in terms of gauge couplings in the MSSM, and the mass parameters can be expressed by the two vacuum expectation values of the neutral Higgs fields and one of the physical Higgs masses. Since the sum of the squares of the vacuum expectation values is given by the W mass, $\tan\beta$, the ratio of the two vacuum expectation values, and M_A , the mass of the CP-odd Higgs boson A , are generally chosen as the free parameters of the MSSM. The trilinear and quartic Higgs self-couplings are determined by those two parameters.

The measurement of the Higgs self-couplings will be a very difficult task. In the Standard Model the production cross section for HH Higgs pairs are small, similarly the continuum production of Higgs pairs in the MSSM. Only if heavy MSSM Higgs bosons can decay into pairs of light Higgs bosons, the associated Higgs self-couplings can be determined fairly easily by measuring the decay branching ratios. Several aspects of multi-Higgs production have been discussed in the literature. Most analyses treat HH pair production in the Standard Model only at the theoretical level [3, 4]. Within the MSSM, the search for the heavy Higgs boson H has been simulated in the $b\bar{b}$ decay mode at the LHC [5]. $h \rightarrow AA$ events have been searched at LEP [6]; more general aspects of multi-Higgs production in e^+e^- collisions have only recently been analyzed theoretically in Ref.[2].

Several mechanisms give rise to the production of pairs of neutral Higgs bosons in hadron collisions. Multi-Higgs final states can be produced through Higgs-strahlung off W bosons and through WW fusion in proton-proton collisions. Bremsstrahlung of Higgs particles off heavy quarks can also be exploited. In the present paper we discuss the production of Higgs pairs in gluon-gluon collisions at the LHC. We have determined the cross sections for the continuum in the Standard Model

$$pp \rightarrow gg \rightarrow HH \quad (1)$$

as well as for the continuum and resonance decays in the minimal supersymmetric theory

$$pp \rightarrow gg \rightarrow \Phi_i \Phi_j \quad \Phi_i = h, H, A \quad (2)$$

¹Following standard notations we have taken care that no confusion will arise from using the same symbol for the SM and the heavy CP-even MSSM Higgs particle.

restricting ourselves to neutral Higgs bosons in the present report². It can be anticipated from the large number of low- x gluons in high-energy proton beams that the gg channel is of particular interest in the continuum for fairly low Higgs masses. In the MSSM the on-shell production of heavy Higgs bosons with subsequent Higgs cascade decays will eventually provide a copious source of light multi-Higgs final states. The cross sections are affected, besides the normal Higgs–boson couplings to gauge bosons and fermions [7], by the trilinear Higgs couplings [8]:

$$\begin{aligned}
SM & : \lambda_{HHH} = \frac{3M_H^2}{M_Z^2} \\
MSSM & : \lambda_{hhh} = 3 \cos(2\alpha) \sin(\beta + \alpha) + \frac{3\epsilon}{M_Z^2} \frac{\cos^3 \alpha}{\sin \beta} \\
& \lambda_{Hhh} = 2 \sin(2\alpha) \sin(\beta + \alpha) - \cos(2\alpha) \cos(\beta + \alpha) + \frac{3\epsilon}{M_Z^2} \frac{\sin \alpha \cos^2 \alpha}{\sin \beta} \\
& \lambda_{HHh} = -2 \sin(2\alpha) \cos(\beta + \alpha) - \cos(2\alpha) \sin(\beta + \alpha) + \frac{3\epsilon}{M_Z^2} \frac{\sin^2 \alpha \cos \alpha}{\sin \beta} \\
& \lambda_{HHH} = 3 \cos(2\alpha) \cos(\beta + \alpha) + \frac{3\epsilon}{M_Z^2} \frac{\sin^3 \alpha}{\sin \beta} \\
& \lambda_{hAA} = \cos(2\beta) \sin(\beta + \alpha) + \frac{\epsilon}{M_Z^2} \frac{\cos \alpha \cos^2 \beta}{\sin \beta} \\
& \lambda_{HAA} = -\cos(2\beta) \cos(\beta + \alpha) + \frac{\epsilon}{M_Z^2} \frac{\sin \alpha \cos^2 \beta}{\sin \beta} \tag{4}
\end{aligned}$$

The couplings in the SM as well as the MSSM are normalized to $\lambda_0 = [\sqrt{2}G_F]^{1/2} M_Z^2$. The MSSM couplings depend on β and the mixing angle α

$$\tan 2\alpha = \frac{M_A^2 + M_Z^2}{M_A^2 - M_Z^2 + \epsilon / \cos 2\beta} \tan 2\beta \tag{5}$$

in the CP-even Higgs sector; radiative corrections have been included in the leading m_t^4 one-loop approximation, parametrized by

$$\epsilon = \frac{3G_F}{\sqrt{2}\pi^2} \frac{m_t^4}{\sin^2 \beta} \log \left[1 + \frac{M_S^2}{m_t^2} \right] \tag{6}$$

with the common squark mass fixed to $M_S = 1$ TeV. In our numerical analysis we have included the leading two-loop corrections to the MSSM Higgs masses and couplings, taken from Ref.[9]. The behaviour of the couplings with M_A is shown for two representative values of $\tan \beta = 1.5$ and 30 in Fig.1.

²The derivation of the SM cross sections has nicely been described in Ref.[4]. We will briefly discuss this case again to exemplify the techniques for the simplest scenario of Higgs pair production, before generalizing the analysis for unequal masses and pseudoscalar Higgs particles in the MSSM.

The paper is organized as follows. In the next section HH pair production through gluon collisions will be discussed in the Standard Model. In the third section we will present the results for all pair combinations of neutral Higgs bosons in the MSSM. Phenomenological aspects including Higgs–strahlung and WW fusion will be presented in a sequel to this paper [10].

2 Higgs Pair Production in the Standard Model

Two mechanisms contribute to the production of Higgs pairs through gg collisions in the Standard Model, exemplified by the generic diagrams in Fig.2a/b. (i) Virtual Higgs bosons which subsequently decay into HH final states, are coupled to gluons by the usual heavy–quark triangle [11, 12]. (ii) The coupling is also mediated by heavy–quark box diagrams.

In the triangle diagram Fig.2a the gluons are coupled to the total spin $S_z = 0$ along the collision axis. The transition matrix element associated with this mechanism can therefore be expressed by the product of one (gauge invariant) form factor F_Δ , depending on the scaling variable $\tau_Q = 4m_Q^2/\hat{s}$, and the generalized coupling C_Δ defined as

$$C_\Delta = \lambda_{HHH} \frac{M_Z^2}{\hat{s} - M_H^2} \quad (7)$$

The coefficient λ_{HHH} denotes the trilinear self-coupling HHH in the Standard Model, cf. eq.(3). \hat{s} is the square of the invariant energy flow through the virtual Higgs line. The well-known form factor F_Δ [11, 12] is given in Appendix A1.

The box diagrams in Fig.2b allow for $S_z = 0$ and 2 gluon–gluon couplings so that the transition matrix element can be expressed in terms of two (gauge invariant) form factors F_\square and G_\square . Fairly compact expressions of the form factors are given in Appendix A1 where the Higgs masses have to be specified to $M_c = M_d = M_H$. The couplings between the Higgs bosons and the quarks are normalized to unity by definition,

$$C_\square = 1 \quad (8)$$

[The overall normalization is included in the prefactors of the cross section and the form factors.] The form factors obtained in this way for the simplified case of equal masses agree with the results in Ref.[4].

In the two limits of light and heavy Higgs bosons with respect to the loop quark mass, very simple expressions can be derived for the three form factors F_Δ and F_\square , G_\square .

(i) Large Quark Mass Limit

The form factors can be evaluated either by taking the limit $m_Q^2 \gg \hat{s} \sim M_H^2$ in the Feynman amplitude or, equivalently, by exploiting the elegant low-energy theorem

$F_{\square} = m_Q^2 \partial(F_{\Delta}/m_Q)/\partial m_Q$ [12–14] for external light scalar Higgs bosons. This reduces the complexity of the calculation considerably:

$$F_{\Delta} = \frac{2}{3} + \mathcal{O}\left(\hat{s}/m_Q^2\right) \quad (9)$$

and

$$\begin{aligned} F_{\square} &= -\frac{2}{3} + \mathcal{O}\left(\hat{s}/m_Q^2\right) \\ G_{\square} &= \mathcal{O}\left(\hat{s}/m_Q^2\right) \end{aligned} \quad (10)$$

Both $S_z = 0$ form factors F_{Δ} and F_{\square} survive in this limit, whereas the $S_z = 2$ form factor G_{\square} vanishes asymptotically.

(ii) Small Quark Mass Limit

In the limit of light quark masses compared with the invariant energy³, large logarithms of the light quark mass $\log \hat{s}/m_Q^2$ will occur in the form factors. Detailed inspection of the Feynman amplitudes leads to the following final expressions:

$$F_{\Delta} = -\frac{m_Q^2}{\hat{s}} \left[\log\left(\frac{m_Q^2}{\hat{s}}\right) + i\pi \right]^2 + \mathcal{O}\left(\frac{m_Q^2}{\hat{s}}\right) \quad (11)$$

and

$$\begin{aligned} F_{\square} &= \mathcal{O}\left(m_Q^2/\hat{s}\right) \\ G_{\square} &= \mathcal{O}\left(m_Q^2/\hat{s}\right) \end{aligned} \quad (12)$$

All form factors vanish to $\mathcal{O}(m_Q^2)$ in this limit since they are suppressed by the Yukawa coupling $\propto m_Q$; this is well-known for the quark triangle. [This limit is not of much practical use in the SM; yet it will be relevant later in the MSSM where b -quark loops are dominant for large $\tan\beta$.]

The differential parton cross section can finally be written in the form

$$\frac{d\hat{\sigma}(gg \rightarrow HH)}{d\hat{t}} = \frac{G_F^2 \alpha_s^2}{256(2\pi)^3} \left[|C_{\Delta} F_{\Delta} + C_{\square} F_{\square}|^2 + |C_{\square} G_{\square}|^2 \right] \quad (13)$$

where \hat{t} is the momentum transfer squared from one of the gluons in the initial state to one of the Higgs bosons in the final state. The total cross section for HH Higgs

³In the leading logarithmic approximation the scale is set effectively by the Higgs mass since the invariant energy $\sqrt{\hat{s}}$ is of the same order as M_H for the cross sections we shall study.

pair production through gg in pp collisions⁴ can be derived by integrating (13) over the scattering angle and the gg luminosity

$$\sigma(pp \rightarrow gg \rightarrow HH) = \int_{4M_H^2/s}^1 d\tau \frac{d\mathcal{L}^{gg}}{d\tau} \hat{\sigma}(\hat{s} = \tau s) \quad (14)$$

This cross section has been evaluated numerically. The analysis has been carried out for the LHC c.m. energy $\sqrt{s} = 14$ TeV; the top quark mass has been set to $m_t = 175$ GeV [15]. The result is shown in Fig.3. For SM Higgs masses close to $M_H \sim 100$ GeV the cross section is of order 10 fb . However, it drops rapidly with increasing Higgs mass; this is a consequence of the fast fall-off of the gg luminosity with rising τ [which is of the order of x_g^2 in the pp collisions]. Nevertheless, at $M_H \sim 100$ GeV order 2,000 events will be produced for an integrated luminosity of $\int \mathcal{L} = 100 \text{ fb}^{-1}$, giving rise to $4b$ and $bb\tau\tau$ final states with large transverse momenta.

3 Neutral Higgs Pairs of the MSSM

A large variety of neutral Higgs pairs of the MSSM can be produced in gluon–gluon collisions:

$$pp \rightarrow gg \rightarrow hh, hH, HH, hA, HA, AA \quad (15)$$

The analysis of the cross sections is in general much more involved than in the SM for two reasons. First, the masses of the two Higgs bosons in the final state are in general different, and second, besides pairs of CP–even Higgs bosons, also pairs of CP–odd and mixed CP–even/CP–odd pairs can be produced.

a) Pairs of CP–even Higgs bosons hh, hH, HH

The mechanisms for the production of CP–even MSSM Higgs bosons $gg \rightarrow H_i H_j$ ($H_i = h, H$) are similar to the Standard Model. The generic triangle and box diagrams are shown in Figs.4a/b. All possible combinations of light and heavy Higgs bosons h and H can be coupled in 3–particle vertices.

The matrix element of the triangle contributions can be expressed in terms of the form factor F_Δ , given in Appendix A1, and the couplings

$$C_\Delta = C_\Delta^h + C_\Delta^H \quad (16)$$

with

$$C_\Delta^{h/H} = \lambda_{H_i H_j(h/H)} \frac{M_Z^2}{\hat{s} - M_{h/H}^2 + iM_{h/H}\Gamma_{h/H}} g_Q^{h/H} \quad (H_i = h, H) \quad (17)$$

The couplings $g_Q^{h/H}$ denote the Higgs–quark couplings in units of the SM Yukawa coupling $[\sqrt{2}G_F]^{1/2}m_Q$. They are collected in Table 1. The Higgs self couplings $\lambda_{H_i H_j(h/H)}$ can be read off eq.(4).

⁴In analogy to single Higgs production via gluon fusion, QCD corrections are expected to enhance the event rate significantly. However, they are known only for the triangle [12] and not for the box; therefore they are not taken into account in the numerical analysis.

Φ		g_t^Φ	g_b^Φ
SM	H	1	1
MSSM	h	$\cos \alpha / \sin \beta$	$-\sin \alpha / \cos \beta$
	H	$\sin \alpha / \sin \beta$	$\cos \alpha / \cos \beta$
	A	$1/\tan \beta$	$\tan \beta$

Table 1: *Higgs couplings in the MSSM to fermions relative to SM couplings.*

For the box contributions we obtain analogous expressions, with two independent form factors F_\square and G_\square contributing. Their expressions can be found in Appendix A1. The corresponding couplings C_\square are built up by the Higgs–quark couplings,

$$C_\square = g_Q^{H_i} g_Q^{H_j} \quad (18)$$

The two limiting cases in which the Higgs masses are either much smaller or much larger than the loop quark masses, are both physically relevant in this case since the top quark as well as the bottom quark play a role, with $M_h^2 \ll m_t^2$ and $M_H^2 \gg m_b^2$. The limits of the form factors are the same as for the SM Higgs bosons eqs.(9–12).

From the differential parton cross section, which includes t and b quark loops,

$$\frac{d\hat{\sigma}(gg \rightarrow H_i H_j)}{d\hat{t}} = \frac{G_F^2 \alpha_s^2}{256(2\pi)^3} \left[\left| \sum_{t,b} (C_\Delta F_\Delta + C_\square F_\square) \right|^2 + \left| \sum_{t,b} C_\square G_\square \right|^2 \right] \quad (19)$$

the pp cross section can be derived by integrating over the scattering angle and attaching the gluon luminosity. The result of the numerical analysis is shown for the final states hh , hH and HH in Figs.5a/b/c for two representative values $\tan \beta = 1.5$ and 30. [Mixing in the stop sector is not taken into account.]

The final state hh deserves special attention. The cross section for moderate values M_h is large since the heavy CP-even Higgs boson H can decay into the two light Higgs bosons (dashed lines). H is produced directly in gg collisions, coupled through the quark triangle, so that the matrix element involves one power of the electroweak coupling less than continuum Higgs pair production. Except for a dip due to a zero in the Hhh coupling λ_{Hhh} , the cross section in the resonance range is of order 10^3 to $10^4 fb$, dropping to the typical hh continuum value of $30 fb$ for increasing H Higgs masses. For $\tan \beta = 1.5$ the curve shows a sharp threshold behavior for $M_H \sim 2m_t$ due to on-shell top pair production in the dominant top quark triangle and, moreover, due to the sharp fall-off of the branching ratio $BR(H \rightarrow hh)$. The cross section for $\tan \beta = 30$ depends strongly on the Higgs boson masses, because resonance production $gg \rightarrow H \rightarrow hh$ is kinematically forbidden for $110 \text{ GeV} \lesssim M_A \lesssim 210 \text{ GeV}$. Above this range this channel opens up again

with a small branching ratio $\sim 10^{-3}$ giving rise to the small bump in the cross section at $M_A \sim 210$ GeV.

The cross sections for hH and HH final states are much smaller, cf. Figs.5b/c. This is the result of the absence of any resonance effect and the phase space suppression due to the large Higgs masses in the final states. The cross section for $pp \rightarrow gg \rightarrow hH$ depends strongly on $\text{tg}\beta$ and it varies between very small values and ~ 100 fb if the entire Higgs mass range is swept. For $\text{tg}\beta = 1.5$ the Higgs mass dependence is smooth, whereas for $\text{tg}\beta = 30$ a sharp peak develops at $M_A \sim 100$ GeV due to the strong variation of the MSSM couplings in this region. At large Higgs masses the cross section decreases strongly with increasing $\text{tg}\beta$. A similar picture emerges for the pair production of heavy scalar Higgs bosons $pp \rightarrow gg \rightarrow HH$. Its size increases at large Higgs masses for increasing $\text{tg}\beta$, where the bottom quark loops become dominant. The strong variation of the cross section for $M_A \sim 100$ GeV and $\text{tg}\beta = 30$ is again due to the rapidly changing MSSM couplings in this mass range.

b) Mixed CP–even/CP–odd pairs

The analysis of the CP–mixed hA and HA final states is in many aspects different from the previous cases. First of all, the final state can be produced through the decay of a virtual Z boson as shown in the generic diagrams of Fig.6. By evaluating the Feynman diagrams one finds the following generalized charges [$H_i = h, H$]

(i) s -channel A exchange:

$$C_{\Delta}^A = \lambda_{AAH_i} \frac{M_Z^2}{\hat{s} - M_A^2 + iM_A\Gamma_A} g_Q^A \quad (20)$$

(ii) s -channel Z exchange:

$$C_{\Delta}^Z = \lambda_{ZAH_i} \frac{M_Z^2}{\hat{s} - M_Z^2 + iM_Z\Gamma_Z} a_Q \quad (21)$$

where $a_Q = 1(-1)$ for top (bottom) quarks denotes the axial charge of the heavy loop quark Q [note that only the Z axial coupling of the heavy loop quark can contribute], and the trilinear couplings λ_{ZAH_i} are given by

$$\begin{aligned} \lambda_{ZAh} &= -\cos(\beta - \alpha) \\ \lambda_{ZAH} &= \sin(\beta - \alpha) \end{aligned} \quad (22)$$

(iii) box contributions:

$$C_{\square}^{AH_i} = g_Q^A g_Q^{H_i} \quad (23)$$

The expressions of the form factors $F_{\Delta}^{A/Z}$ and F_{\square} , G_{\square} can be found in Appendix A2.

In analogy to the CP–even case, simple expressions can be derived for the form factors in the limits of large and small Higgs masses compared with the quark masses.

(i) Large Quark Mass Limit

The triangular form factor can be derived in this limit from the axial anomaly. The box form factor is given by the derivative of the anomaly $F_{\square} = m_Q^2 \partial(F_{\Delta}^A/m_Q)/\partial m_Q$ [12, 14]. Simple expressions can be obtained:

$$\begin{aligned} F_{\Delta}^A &= 1 + \mathcal{O}\left(\hat{s}/m_Q^2\right) \\ F_{\Delta}^Z &= \mathcal{O}\left(\hat{s}/m_Q^2\right) \end{aligned} \quad (24)$$

and

$$\begin{aligned} F_{\square} &= -1 + \mathcal{O}\left(\hat{s}/m_Q^2\right) \\ G_{\square} &= \mathcal{O}\left(\hat{s}/m_Q^2\right) \end{aligned} \quad (25)$$

(ii) Small Quark Mass Limit

$$\begin{aligned} F_{\Delta}^A &= -\frac{m_Q^2}{\hat{s}} \left[\log\left(\frac{m_Q^2}{\hat{s}}\right) + i\pi \right]^2 + \mathcal{O}\left(\frac{m_Q^2}{\hat{s}}\right) \\ F_{\Delta}^Z &= \frac{\hat{s} - M_Z^2}{\hat{s}} \frac{M_{H_i}^2 - M_A^2}{M_Z^2} \left\{ 1 + \frac{m_Q^2}{\hat{s}} \left[\log\left(\frac{m_Q^2}{\hat{s}}\right) + i\pi \right]^2 + \mathcal{O}\left(\frac{m_Q^2}{\hat{s}}\right) \right\} \\ F_{\square} &= \mathcal{O}\left(m_Q^2/\hat{s}\right) \\ G_{\square} &= \mathcal{O}\left(m_Q^2/\hat{s}\right) \end{aligned} \quad (26)$$

The differential parton cross section is determined by the form factors, including t and b quark loops:

$$\frac{d\hat{\sigma}(gg \rightarrow AH_i)}{d\hat{t}} = \frac{G_F^2 \alpha_s^2}{256(2\pi)^3} \left[\left| \sum_{t,b} (C_{\Delta} F_{\Delta} + C_{\square} F_{\square}) \right|^2 + \left| \sum_{t,b} C_{\square} G_{\square} \right|^2 \right] \quad (27)$$

The results of the numerical analysis of the two pp cross sections are shown in Figs.7a/b. For light masses M_h the invariant mass [hA] of the final state is small so that the cross section is enhanced by the large phase space. For large Higgs masses the cross section decreases strongly with increasing $\tan\beta$ and drops to a level of about 10^{-1} to $10^{-3} fb$ at $M_A \sim 1$ TeV, where it cannot be observed anymore. The strong variation for $\tan\beta = 30$ at $M_A \sim 100$ GeV is generated by the rapid change of the MSSM couplings with M_A .

Due to the larger mass of the heavy scalar Higgs boson H , the cross section for HA production turns out to be smaller than for hA production.

c) AA pairs of CP-odd Higgs bosons

This case is again closely related to the CP-even pairs. In the box diagrams, Fig.8b, some terms flip just the sign when the $\gamma_5 \times \gamma_5$ couplings are reduced to $\mathbb{1}$ in the loop trace. As a result, the matrix elements can be expressed in terms of the couplings

$$C_{\Delta} = C_{\Delta}^h + C_{\Delta}^H \quad (28)$$

with

$$\begin{aligned} C_{\Delta}^{h/H} &= \lambda_{AA(h/H)} \frac{M_Z^2}{\hat{s} - M_{h/H}^2 + iM_{h/H}\Gamma_{h/H}} g_Q^{h/H} \\ C_{\square} &= (g_Q^A)^2 \end{aligned} \quad (29)$$

The form factors F_{Δ} for the triangle contributions and F_{\square}, G_{\square} for the box contribution can be found in Appendix A3 by choosing $M_c = M_d = M_A$.

In the limits of large and small Higgs masses compared with the quark masses simple expressions can be derived.

(i) Large Quark Mass Limit

The triangle form factor coincides with the scalar expression eq.(9), and the box form factor can be obtained from the derivative of the gluon self-energy $[\mathcal{M}(ggA^2) = \sqrt{2}G_F m_Q \partial \mathcal{M}(gg)/\partial m_Q]$ [14] leading to the results

$$F_{\Delta} = \frac{2}{3} + \mathcal{O}(\hat{s}/m_Q^2) \quad (30)$$

and

$$\begin{aligned} F_{\square} &= \frac{2}{3} + \mathcal{O}(\hat{s}/m_Q^2) \\ G_{\square} &= \mathcal{O}(\hat{s}/m_Q^2) \end{aligned} \quad (31)$$

(ii) Small Quark Mass Limit

$$F_{\Delta} = -\frac{m_Q^2}{\hat{s}} \left[\log\left(\frac{m_Q^2}{\hat{s}}\right) + i\pi \right]^2 + \mathcal{O}\left(\frac{m_Q^2}{\hat{s}}\right) \quad (32)$$

and

$$\begin{aligned} F_{\square} &= \mathcal{O}(m_Q^2/\hat{s}) \\ G_{\square} &= \mathcal{O}(m_Q^2/\hat{s}) \end{aligned} \quad (33)$$

The pp cross section is shown in Fig.9. The large value of the cross section for small A masses is due to resonance $H \rightarrow AA$ decays. When this channel is closed, the cross section becomes more and more suppressed with rising A mass in the final state. For $\text{tg}\beta = 1.5$ the cross section develops a kink at the $(t\bar{t})$ threshold $M_A = 2m_t$ due to S -wave $(t\bar{t})$ -resonance production. Above this mass value the phase space suppression leads to a rapidly decreasing cross section, to a level of $\sim 10^{-3} \text{fb}$ at $M_A \sim 1 \text{ TeV}$. For $\text{tg}\beta = 30$ the bottom quark loops are dominant so that the cross section depends smoothly on M_A . For large pseudoscalar masses the signal increases with increasing $\text{tg}\beta$.

4 Appendices

A1. Form factors for two scalar Higgs bosons $g_a g_b \rightarrow H_c H_d$

notation:

parameter definitions:

$$\begin{aligned} \hat{s} &= (p_a + p_b)^2, & \hat{t} &= (p_c - p_a)^2, & \hat{u} &= (p_c - p_b)^2 \\ S &= \hat{s}/m_Q^2, & T &= \hat{t}/m_Q^2, & U &= \hat{u}/m_Q^2 \\ \rho_c &= M_c^2/m_Q^2, & \rho_d &= M_d^2/m_Q^2, & \tau_Q &= 4/S \\ T_1 &= T - \rho_c, & U_1 &= U - \rho_c, & T_2 &= T - \rho_d, & U_2 &= U - \rho_d \end{aligned}$$

Scalar integrals:

$$\begin{aligned} C_{ij} &= \int \frac{d^4 q}{i\pi^2} \frac{1}{(q^2 - m_Q^2) [(q + p_i)^2 - m_Q^2] [(q + p_i + p_j)^2 - m_Q^2]} \\ D_{ijk} &= \int \frac{d^4 q}{i\pi^2} \frac{1}{(q^2 - m_Q^2) [(q + p_i)^2 - m_Q^2] [(q + p_i + p_j)^2 - m_Q^2] [(q + p_i + p_j + p_k)^2 - m_Q^2]} \end{aligned}$$

The analytic expressions can be found in Ref.[16].

triangle form factor:

$$F_\Delta = \frac{2}{S} \left\{ 2 + (4 - S)m_Q^2 C_{ab} \right\} = \tau_Q \left[1 + (1 - \tau_Q)f(\tau_Q) \right]$$

$$f(\tau_Q) = \begin{cases} \arcsin^2 \frac{1}{\sqrt{\tau_Q}} & \tau_Q \geq 1 \\ -\frac{1}{4} \left[\log \frac{1 + \sqrt{1 - \tau_Q}}{1 - \sqrt{1 - \tau_Q}} - i\pi \right]^2 & \tau_Q < 1 \end{cases}$$

box form factors:

$$\begin{aligned}
F_{\square} &= \frac{1}{S^2} \left\{ 4S + 8Sm_Q^2 C_{ab} - 2S(S + \rho_c + \rho_d - 8)m_Q^4 (D_{abc} + D_{bac} + D_{acb}) \right. \\
&\quad + (\rho_c + \rho_d - 8)m_Q^2 \left[T_1 C_{ac} + U_1 C_{bc} + U_2 C_{ad} + T_2 C_{bd} - (TU - \rho_c \rho_d)m_Q^2 D_{acb} \right] \Big\} \\
G_{\square} &= \frac{1}{S(TU - \rho_c \rho_d)} \left\{ (T^2 + \rho_c \rho_d - 8T)m_Q^2 \left[SC_{ab} + T_1 C_{ac} + T_2 C_{bd} - STm_Q^2 D_{bac} \right] \right. \\
&\quad + (U^2 + \rho_c \rho_d - 8U)m_Q^2 \left[SC_{ab} + U_1 C_{bc} + U_2 C_{ad} - SUm_Q^2 D_{abc} \right] \\
&\quad - (T^2 + U^2 - 2\rho_c \rho_d)(T + U - 8)m_Q^2 C_{cd} \\
&\quad \left. - 2(T + U - 8)(TU - \rho_c \rho_d)m_Q^4 (D_{abc} + D_{bac} + D_{acb}) \right\}
\end{aligned}$$

tensor basis:

$$\begin{aligned}
S_z = 0 &: A_1^{\mu\nu} = g^{\mu\nu} - \frac{p_a^\nu p_b^\mu}{(p_a p_b)} \\
S_z = 2 &: A_2^{\mu\nu} = g^{\mu\nu} + \frac{p_c^2 p_a^\nu p_b^\mu}{p_T^2(p_a p_b)} - \frac{2(p_b p_c) p_a^\nu p_c^\mu}{p_T^2(p_a p_b)} - \frac{2(p_a p_c) p_b^\mu p_c^\nu}{p_T^2(p_a p_b)} + \frac{2p_c^\mu p_c^\nu}{p_T^2} \\
\text{with} & \quad p_T^2 = 2 \frac{(p_a p_c)(p_b p_c)}{(p_a p_b)} - p_c^2
\end{aligned}$$

$$A_1 \cdot A_2 = 0, \quad A_1 \cdot A_1 = A_2 \cdot A_2 = 2$$

matrix element:

$$\begin{aligned}
\mathcal{M}(g_a g_b \rightarrow H_c H_d) &= \mathcal{M}_{\triangle}^h + \mathcal{M}_{\triangle}^H + \mathcal{M}_{\square} \\
\mathcal{M}_{\triangle}^{h/H} &= \frac{G_F \alpha_s \hat{s}}{2\sqrt{2}\pi} C_{\triangle}^{h/H} F_{\triangle} A_{1\mu\nu} \epsilon_a^\mu \epsilon_b^\nu \delta_{ab} \\
\mathcal{M}_{\square} &= \frac{G_F \alpha_s \hat{s}}{2\sqrt{2}\pi} C_{\square} (F_{\square} A_{1\mu\nu} + G_{\square} A_{2\mu\nu}) \epsilon_a^\mu \epsilon_b^\nu \delta_{ab}
\end{aligned}$$

A2. Form factors for a mixed scalar–pseudoscalar pair $g_a g_b \rightarrow A_c H_d$

triangle form factor:

$$\begin{aligned}
F_{\triangle}^A &= -2m_Q^2 C_{ab} = \tau_Q f(\tau_Q) \\
F_{\triangle}^Z &= \left(1 - \frac{\hat{s}}{M_Z^2} \right) \frac{\rho_c - \rho_d}{S} \left[1 + 2m_Q^2 C_{ab} \right] = \left(1 - \frac{\hat{s}}{M_Z^2} \right) \frac{\rho_c - \rho_d}{S} \left[1 - \tau_Q f(\tau_Q) \right]
\end{aligned}$$

box form factors:

$$\begin{aligned}
F_{\square} &= \frac{1}{S^2} \left\{ -2S(S + \rho_c - \rho_d)m_Q^4(D_{abc} + D_{bac} + D_{acb}) \right. \\
&\quad + (\rho_c - \rho_d)m_Q^2 \left[T_1 C_{ac} + U_1 C_{bc} + U_2 C_{ad} + T_2 C_{bd} - (TU - \rho_c \rho_d)m_Q^2 D_{acb} \right] \left. \right\} \\
G_{\square} &= \frac{1}{S(TU - \rho_c \rho_d)} \left\{ (U^2 - \rho_c \rho_d)m_Q^2 \left[SC_{ab} + U_1 C_{bc} + U_2 C_{ad} - SU m_Q^2 D_{abc} \right] \right. \\
&\quad - (T^2 - \rho_c \rho_d)m_Q^2 \left[SC_{ab} + T_1 C_{ac} + T_2 C_{bd} - ST m_Q^2 D_{bac} \right] \\
&\quad + \left[(T+U)^2 - 4\rho_c \rho_d \right] (T-U)m_Q^2 C_{cd} \\
&\quad \left. + 2(T-U)(TU - \rho_c \rho_d)m_Q^4(D_{abc} + D_{bac} + D_{acb}) \right\}
\end{aligned}$$

tensor basis:

$$\begin{aligned}
S_z = 0 &: A_1^{\mu\nu} = \frac{1}{(p_a p_b)} \epsilon^{\mu\nu p_a p_b} \\
S_z = 2 &: A_2^{\mu\nu} = \frac{p_c^\mu \epsilon^{\nu p_a p_b p_c} + p_c^\nu \epsilon^{\mu p_a p_b p_c} + (p_b p_c) \epsilon^{\mu\nu p_a p_c} + (p_a p_c) \epsilon^{\mu\nu p_b p_c}}{(p_a p_b) p_T^2} \\
\text{with} & \quad p_T^2 = 2 \frac{(p_a p_c)(p_b p_c)}{(p_a p_b)} - p_c^2
\end{aligned}$$

$$A_1 \cdot A_2 = 0 \quad A_1 \cdot A_1 = A_2 \cdot A_2 = 2$$

matrix element:

$$\begin{aligned}
\mathcal{M}(g_a g_b \rightarrow A_c H_d) &= \mathcal{M}_{\triangle}^A + \mathcal{M}_{\triangle}^Z + \mathcal{M}_{\square} \\
\mathcal{M}_{\triangle}^{A/Z} &= \frac{G_F \alpha_s \hat{s}}{2\sqrt{2}\pi} C_{\triangle}^{A/Z} F_{\triangle}^{A/Z} A_{1\mu\nu} \epsilon_a^\mu \epsilon_b^\nu \delta_{ab} \\
\mathcal{M}_{\square} &= \frac{G_F \alpha_s \hat{s}}{2\sqrt{2}\pi} C_{\square} (F_{\square} A_{1\mu\nu} + G_{\square} A_{2\mu\nu}) \epsilon_a^\mu \epsilon_b^\nu \delta_{ab}
\end{aligned}$$

A3. Form factors for two pseudoscalar Higgs bosons⁵ $\mathbf{g}_a \mathbf{g}_b \rightarrow \mathbf{A}_c \mathbf{A}_d$

triangle form factor:

$$F_{\triangle} = \frac{2}{S} \left\{ 2 + (4-S)m_Q^2 C_{ab} \right\} = \tau_Q \left[1 + (1-\tau_Q)f(\tau_Q) \right]$$

⁵We present the formulae for different masses of the two pseudoscalar particles so that they can also be applied to non-minimal SUSY extensions in which several pseudoscalar particles in general belong to the Higgs spectrum.

box form factors:

$$\begin{aligned}
F_{\square} &= \frac{1}{S^2} \left\{ 4S + 8Sm_Q^2 C_{ab} - 2S(T+U)m_Q^4 (D_{abc} + D_{bac} + D_{acb}) \right. \\
&\quad \left. + (\rho_c + \rho_d)m_Q^2 \left[T_1 C_{ac} + U_1 C_{bc} + U_2 C_{ad} + T_2 C_{bd} - (TU - \rho_c \rho_d)m_Q^2 D_{acb} \right] \right\} \\
G_{\square} &= \frac{1}{S(TU - \rho_c \rho_d)} \left\{ (T^2 + \rho_c \rho_d)m_Q^2 \left[SC_{ab} + T_1 C_{ac} + T_2 C_{bd} - STm_Q^2 D_{bac} \right] \right. \\
&\quad \left. + (U^2 + \rho_c \rho_d)m_Q^2 \left[SC_{ab} + U_1 C_{bc} + U_2 C_{ad} - SUm_Q^2 D_{abc} \right] \right. \\
&\quad \left. - (T^2 + U^2 - 2\rho_c \rho_d)(T+U)m_Q^2 C_{cd} \right. \\
&\quad \left. - 2(T+U)(TU - \rho_c \rho_d)m_Q^4 (D_{abc} + D_{bac} + D_{acb}) \right\}
\end{aligned}$$

tensor basis:

$$\begin{aligned}
S_z = 0 &: \quad A_1^{\mu\nu} = g^{\mu\nu} - \frac{p_a^\nu p_b^\mu}{(p_a p_b)} \\
S_z = 2 &: \quad A_2^{\mu\nu} = g^{\mu\nu} + \frac{p_c^2 p_a^\nu p_b^\mu}{p_T^2(p_a p_b)} - \frac{2(p_b p_c)p_a^\nu p_c^\mu}{p_T^2(p_a p_b)} - \frac{2(p_a p_c)p_b^\mu p_c^\nu}{p_T^2(p_a p_b)} + \frac{2p_c^\mu p_c^\nu}{p_T^2} \\
\text{with} \quad & p_T^2 = 2 \frac{(p_a p_c)(p_b p_c)}{(p_a p_b)} - p_c^2
\end{aligned}$$

$$A_1 \cdot A_2 = 0 \quad A_1 \cdot A_1 = A_2 \cdot A_2 = 2$$

matrix element:

$$\begin{aligned}
\mathcal{M}(g_a g_b \rightarrow A_c A_d) &= \mathcal{M}_{\triangle}^h + \mathcal{M}_{\triangle}^H + \mathcal{M}_{\square} \\
\mathcal{M}_{\triangle}^{h/H} &= \frac{G_F \alpha_s \hat{s}}{2\sqrt{2}\pi} C_{\triangle}^{h/H} F_{\triangle} A_{1\mu\nu} \epsilon_a^\mu \epsilon_b^\nu \delta_{ab} \\
\mathcal{M}_{\square} &= \frac{G_F \alpha_s \hat{s}}{2\sqrt{2}\pi} C_{\square} (F_{\square} A_{1\mu\nu} + G_{\square} A_{2\mu\nu}) \epsilon_a^\mu \epsilon_b^\nu \delta_{ab}
\end{aligned}$$

References

- [1] P.W. Higgs, Phys. Rev. Lett. **12** (1964) 132 and Phys. Rev. **145** (1966) 1156; F. Englert and R. Brout, Phys. Rev. Lett. **13** (1964) 321; G.S. Guralnik, C.R. Hagen and T.W. Kibble, Phys. Rev. Lett. **13** (1964) 585.

- [2] A. Djouadi, H.E. Haber and P.M. Zerwas, Report DESY 95–214.
- [3] W.-Y. Keung, Mod. Phys. Lett. **A2** (1987) 762; D.A. Dicus, K.J. Kallianpur and S.S.D. Willenbrock, Phys. Lett. **B200** (1988) 187; O.J.P. Eboli, G.C. Marques, S.F. Novaes and A.A.Natale, Phys. Lett. **B197** (1987) 269.
- [4] E.W.N. Glover and J.J. van der Bij, Nucl. Phys. **B309** (1988) 282.
- [5] J. Dai, J.F. Gunion and R. Vega, Phys. Rev. Lett. **71** (1993) 2699; D. Froidevaux and E. Richter–Was, Z. Phys. **C67** (1995) 213; J. Dai, J.F. Gunion and R. Vega, Preprint UCD–95–25.
- [6] For a review see J.–F. Grivaz, Proceedings, International Europhysics Conference on High Energy Physics, Brussels 1995.
- [7] See e.g. A. Djouadi, J. Kalinowski and P.M. Zerwas, Report DESY 95–211.
- [8] V. Barger, M. Berger, A. Stange and R. Phillips, Phys. Rev. **D45** (1992) 4128; Z. Kunszt and F. Zwirner, Nucl. Phys. **B385** (1992) 3.
- [9] M. Carena, J. Espinosa, M. Quiros and C.E.M. Wagner, Phys. Lett. **B355** (1995) 209.
- [10] T. Plehn, M. Spira and P.M. Zerwas, in preparation.
- [11] H. Georgi, S. Glashow, M. Machacek and D.V. Nanopoulos, Phys. Rev. Lett. **40** (1978) 692.
- [12] M. Spira, A. Djouadi, D. Graudenz and P.M. Zerwas, Nucl. Phys. **B453** (1995) 17.
- [13] J. Ellis, M.K. Gaillard and D.V. Nanopoulos, Nucl. Phys. **B106** (1976) 292; A.I. Vainshtain, M.B. Voloshin, V.I. Sakharov and M.A. Shifman, Sov. J. Nucl. Phys. **30** (1979) 711.
- [14] B.A. Kniehl and M. Spira, Z. Phys. **C69** (1995) 77.
- [15] A. Menzione, Proceedings, International Europhysics Conference on High Energy Physics, Brussels 1995.
- [16] G. Passarino and M. Veltman, Nucl. Phys. **B160** (1979) 151; B.A. Kniehl, Phys. Rev. **D42** (1990) 3100.
- [17] M. Glück, E. Reya and A. Vogt, Z. Phys. **C53** (1992) 127.
- [18] S. Bethke, Proceedings QCD 94, Montpellier 1994; Report RWTH Aachen, PITHA–94–30.

FIGURE CAPTIONS

Fig.1: Trilinear Higgs couplings in the MSSM as a function of the pseudoscalar Higgs mass M_A for two representative values $\text{tg}\beta = 1.5$ and 30 [no mixing in the stop sector, c.f. Ref.[9]].

Fig.2: Generic diagrams describing SM Higgs pair production in gluon–gluon collisions: a) triangle and b) box contributions.

Fig.3: Total cross section of SM Higgs pair production at the LHC [$\sqrt{s} = 14$ TeV]. The top mass has been chosen to be $m_t = 175$ GeV and the bottom mass $m_b = 5$ GeV. The GRV parametrizations [17] of the parton densities have been adopted. The factorization and renormalization scales are identified with the invariant mass of the Higgs boson pair. The world average value $\alpha_s(M_Z) = 0.118$ [18] has been chosen for the QCD coupling.

Fig.4: Generic diagrams contributing to pair production of CP–even MSSM Higgs bosons in gluon–gluon collisions $gg \rightarrow hh, hH, HH$: a) triangle and b) box contributions.

Fig.5: Total cross sections for pair production of CP–even MSSM Higgs bosons in gluon–gluon collisions at the LHC: a) hh , b) hH and c) HH pair production for $\text{tg}\beta = 1.5$ and 30 . The secondary axes present the scalar Higgs masses $M_{h/H}$ corresponding to the pseudoscalar masses M_A for both values of $\text{tg}\beta$. The same parameters and parton densities as in Fig.3 have been adopted. The dashed curves in Fig.5a represent the resonant contributions $gg \rightarrow H \rightarrow hh$.

Fig.6: Diagram of the Z boson s –channel contribution to mixed CP–even/CP–odd MSSM Higgs pair production in gluon–gluon collisions and box diagram.

Fig.7: Total cross sections for mixed CP–even/CP–odd pair production of MSSM Higgs bosons in gluon–gluon collisions at the LHC for $\text{tg}\beta = 1.5$ and 30 : a) hA and b) HA production. The secondary axes show the scalar Higgs boson masses corresponding to the pseudoscalar mass M_A for both values of $\text{tg}\beta$. The same parameters as in Fig.3 have been chosen.

Fig.8: Generic triangle and box diagrams for pair production of CP–odd MSSM Higgs bosons in gluon–gluon collisions.

Fig.9: Total cross section of CP–odd MSSM Higgs pair production in gluon–gluon collisions at the LHC for $\text{tg}\beta = 1.5$ and 30 . The parameters are the same as in Fig.3. The dashed curves represent the resonant contributions $gg \rightarrow H \rightarrow AA$.

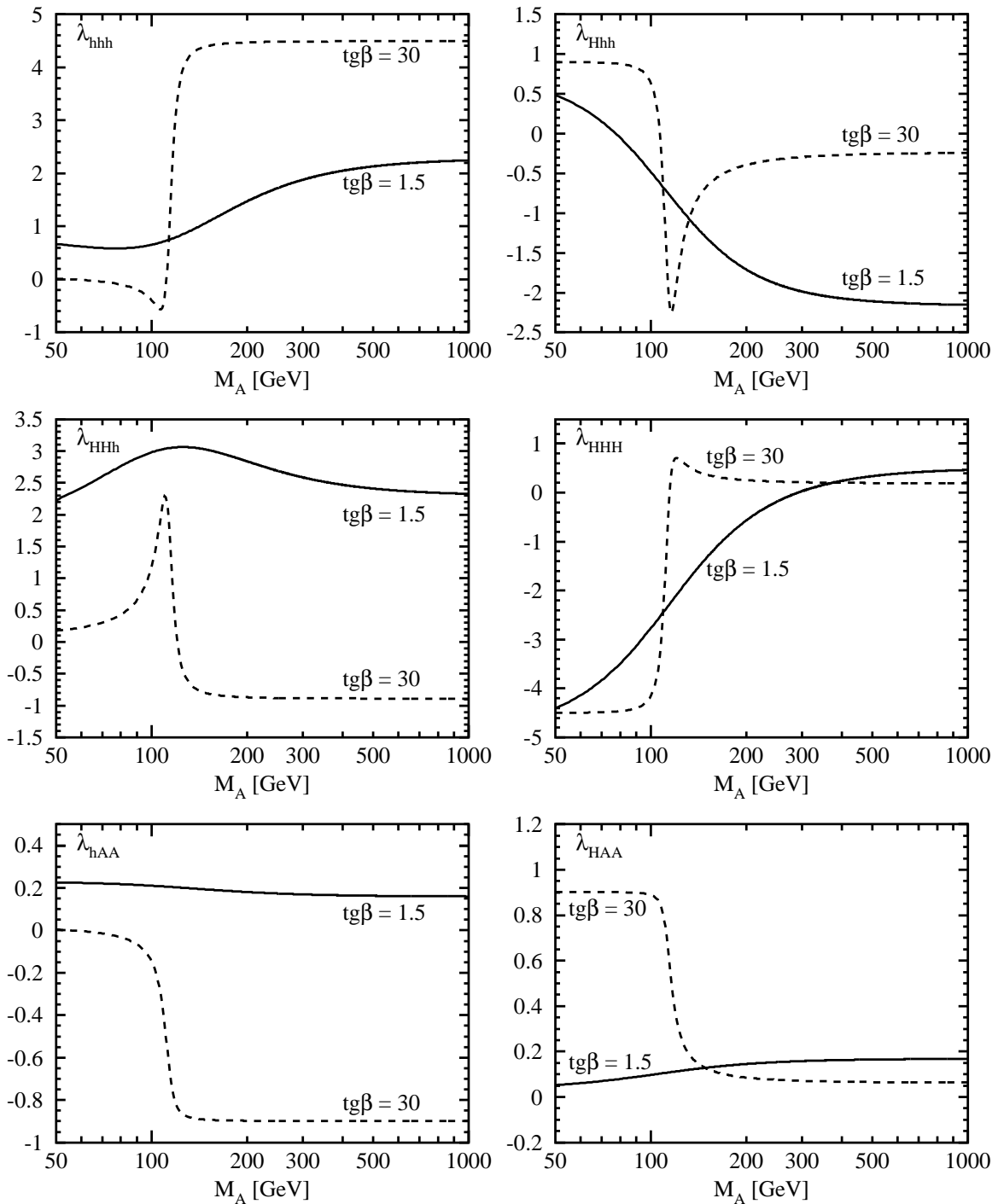


Fig. 1

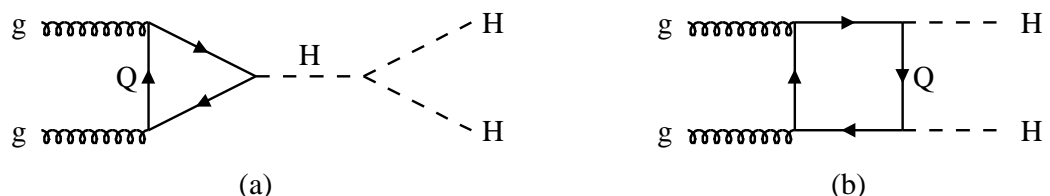


Fig. 2

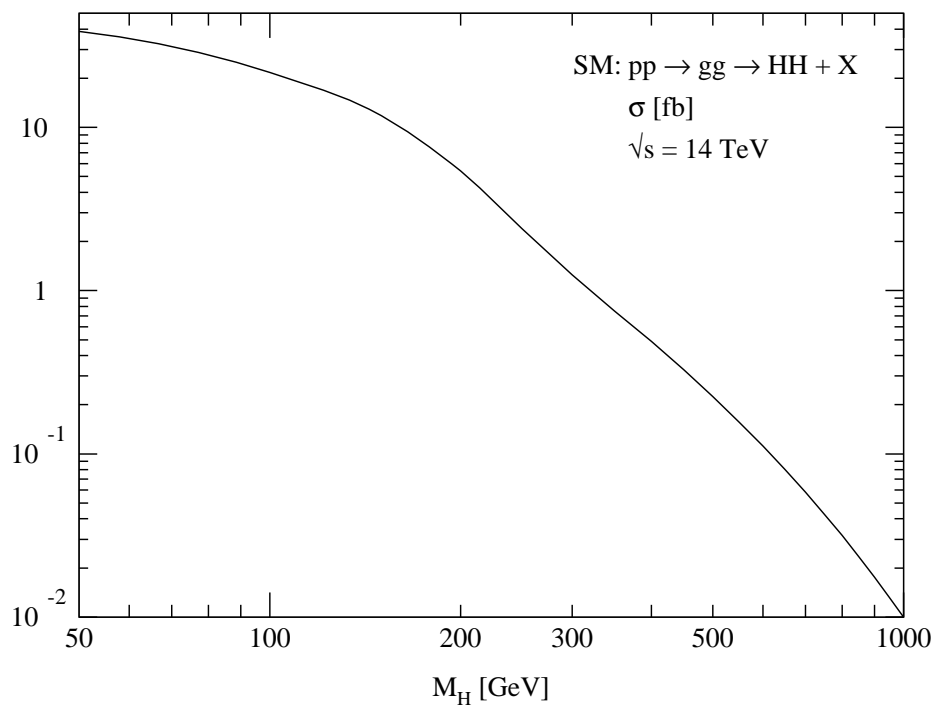


Fig. 3

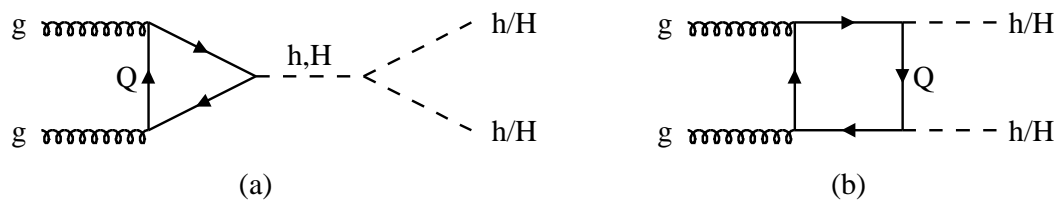


Fig. 4

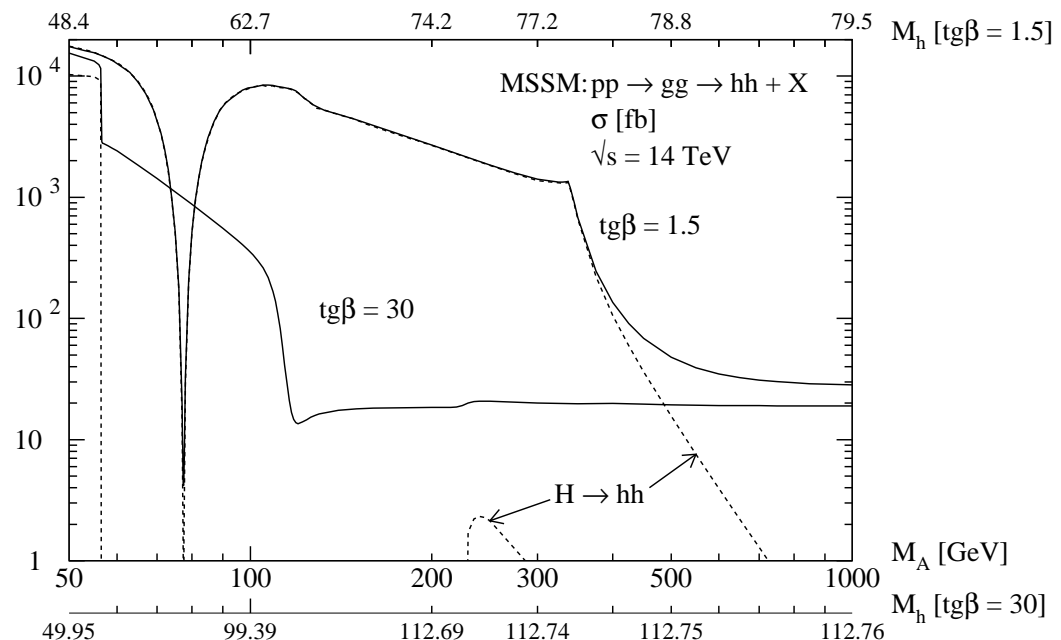


Fig. 5a

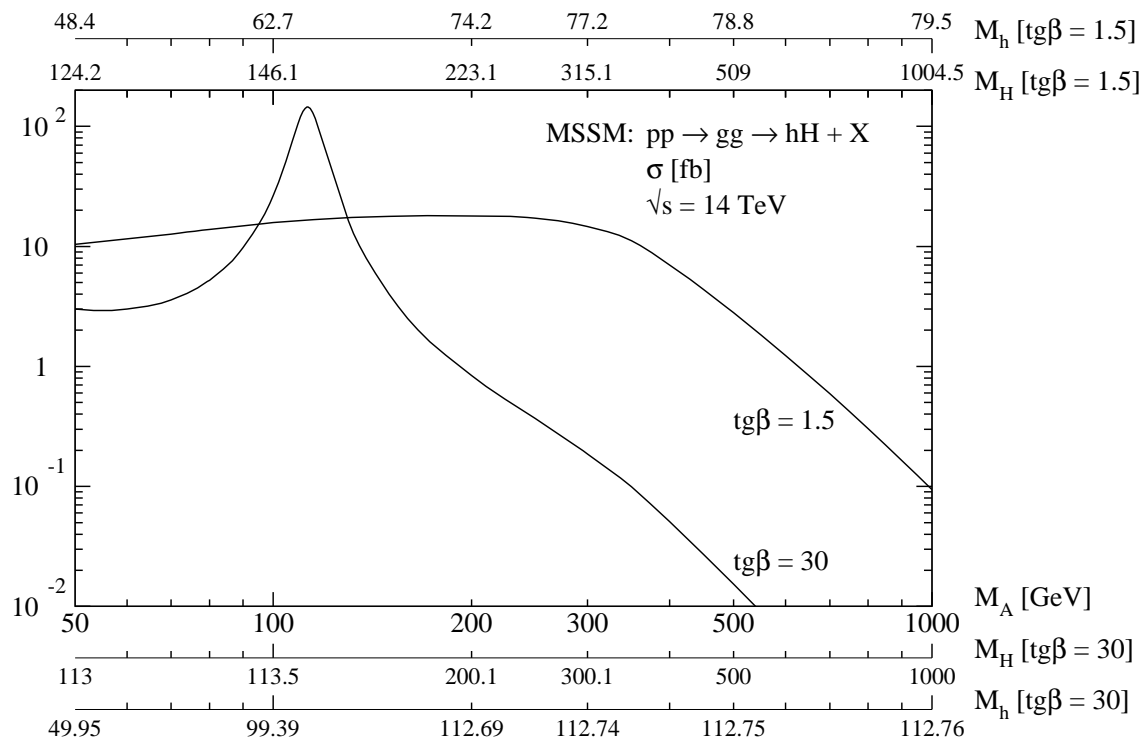


Fig. 5b

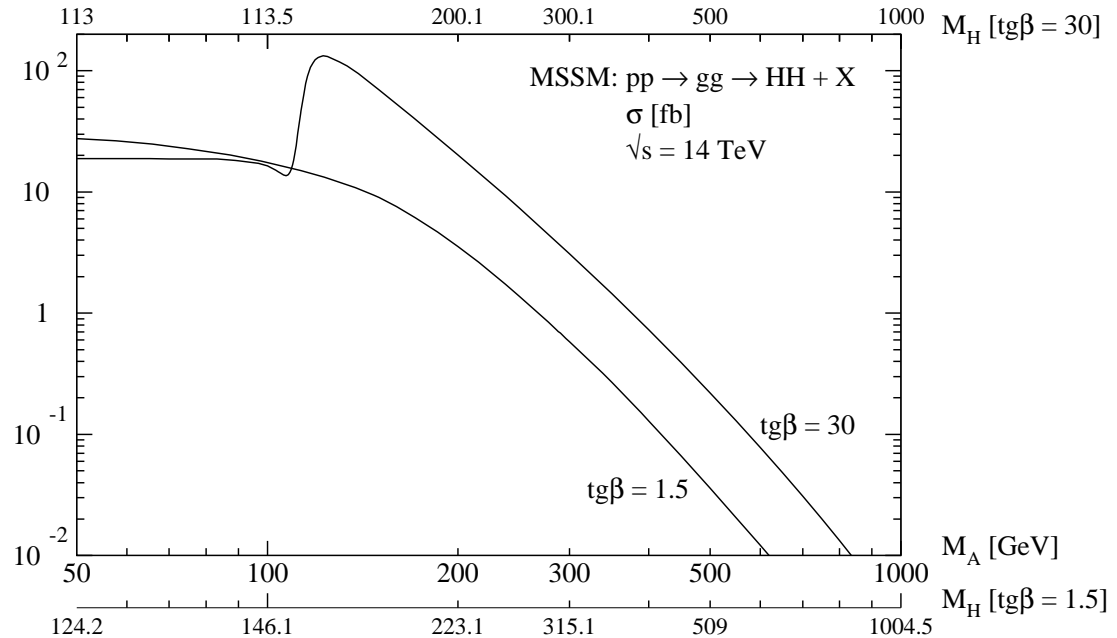


Fig. 5c

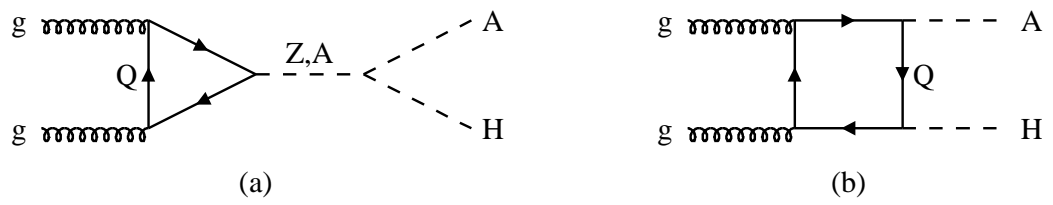


Fig. 6

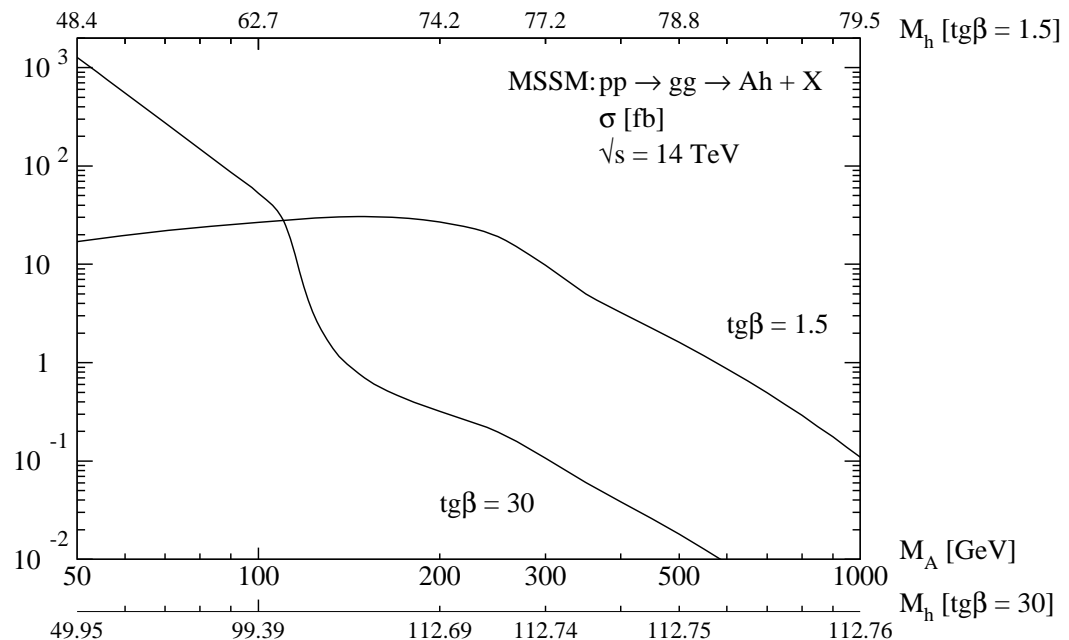


Fig. 7a

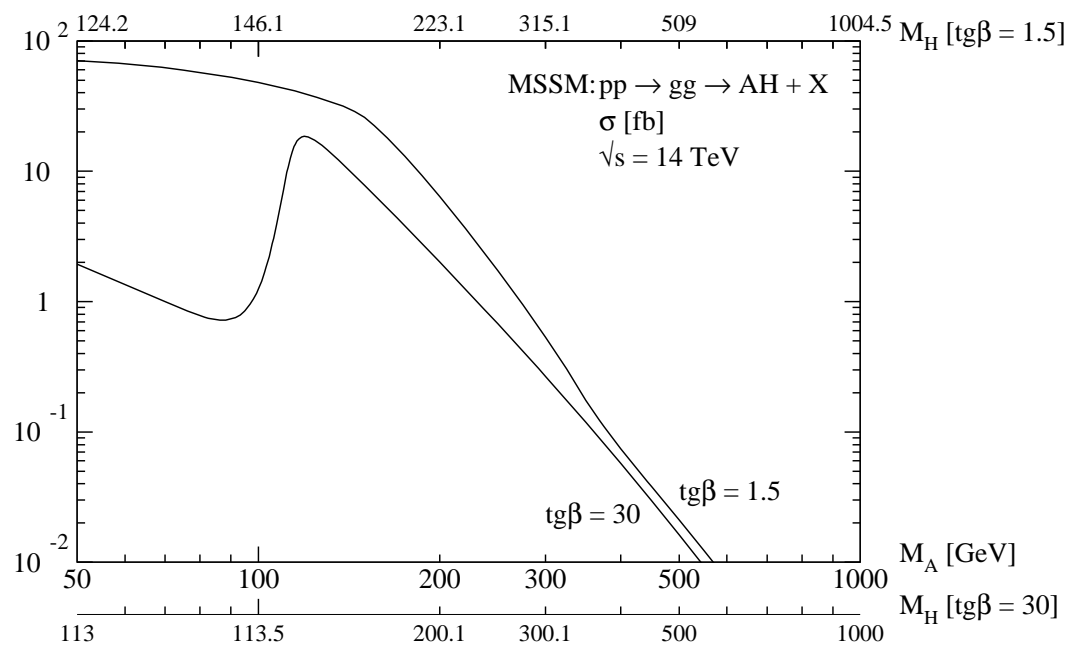


Fig. 7b

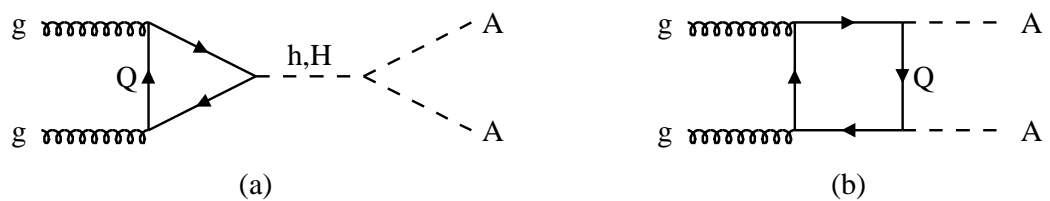


Fig. 8

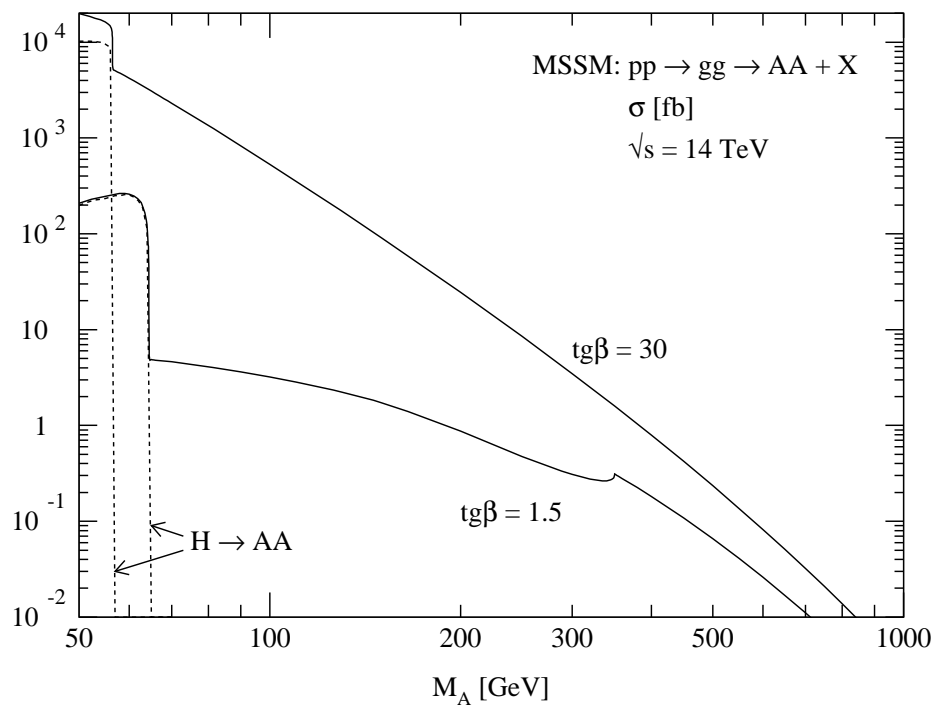


Fig. 9